

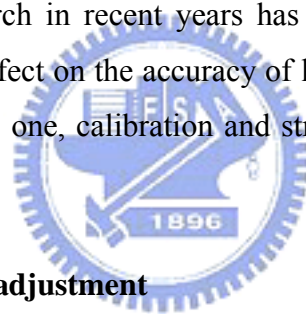
CHAPTER 3

MOTIVATION

The first section of this chapter reviews the previous work on recovering the calibration parameters and assessing the quality of ALS data. The subsequent section outlines the contribution of the current research to this topic.

3.1 Review of previous work

A growing field of research in recent years has identified the existence of systematic errors in ALS data and their effect on the accuracy of laser data. This field of research can be categorized into two subfields: one, calibration and strip adjustment, and two, data accuracy assessment.



3.1.1 Calibration and strip adjustment

Kilian et al. (1996) developed an approach which treats calibration of the laser strips as a block adjustment. The corresponding locations are established between laser points and distinct landmarks (such as building corners) based on a point-based approach. The tie zones from neighboring strips are matched by a Least Squares Matching (LSM) algorithm, where the three adjusted parameters between tie zones are dx , dy , dz (also known as the offsets). Distinct landmarks are used as 3-D control points and flat surfaces as elevation control.

The mathematical model used by Kilian et al. (1996) in analyzing a linear drift examines two aspects: position and attitudes. For each strip, a total of twelve unknown transformation parameters needs to be estimated. As shown in equation 3-1,

$$\begin{aligned}
dX &= \Delta X + v_x + f((\Delta\omega + v_\omega), (\Delta\varphi + v_\varphi), (\Delta\kappa + v_\kappa)) \\
dY &= \Delta Y + v_y + f((\Delta\omega + v_\omega), (\Delta\varphi + v_\varphi), (\Delta\kappa + v_\kappa)) \\
dZ &= \Delta Z + v_z + f((\Delta\omega + v_\omega), (\Delta\varphi + v_\varphi), (\Delta\kappa + v_\kappa))
\end{aligned} \tag{3-1}$$

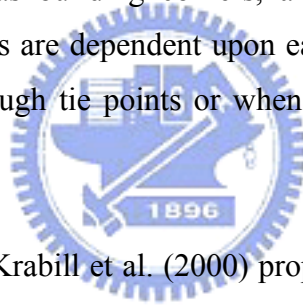
where,

$\Delta X, \Delta Y, \Delta Z$: representing an offset for the translation parameters,

$\Delta\omega, \Delta\varphi, \Delta\kappa$: representing an offset for roll, pitch and heading,

$v_x, v_y, v_z, v_\omega, v_\varphi, v_\kappa$: representing a time-dependent drift

The drawback of this approach is the choice of objects that are used as control points. As the airborne laser scanners sample the surface, the probability that a corner or an edge is sampled is low. Consequently, the differences calculated are based on interpolation. Therefore, the corners of objects, such as building corners, are less accurate laser points. Another drawback is that the parameters are dependent upon each other. Thus, the resulting accuracy is low when there are not enough tie points or when the selected tie points are not evenly distributed.



Vaughn et al. (1996) and Krabill et al. (2000) proposed an in-flight boresight calibration by flying over a locally leveled surface (e.g. a water body) or a well-known surface. Pitch and roll maneuvers are carried out to determine the calibration parameters. The only systematic error recovered is the mounting bias between the laser range finder and the IMU.

The calibration parameters are computed by plotting the roll or pitch versus the measurement range. Therefore, the range variation as a function of the pitch and roll angles takes a concave shape. Second-degree polynomials are fitted to both of these shapes. Their minima are considered as the mounting bias. The biases are then used to update the pitch and roll angles; the process is repeated until convergence is reached. According to the authors, convergence is reached whenever the mounting bias is less than 1 degree. A flat locally horizontal plane is used as a reference surface.

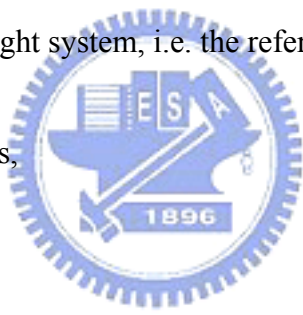
In Crombaghs et al. (2000), trends of height disagreements between adjacent laser scanning strips and with respect to ground control points (GCPs) have been estimated. The mathematical model assumes a vertical translation and two rotations (i.e. roll and pitch misalignment) for each strip. The difference between overlapping strips is modeled with a three-parameter surface, i.e.

$$\begin{aligned} H_{ki}^{laser} - H_{ji}^{laser} &= a_j + b_j U_{ji} + c_j V_{ji} - a_k - b_k U_{ki} - c_k V_{ki} \\ H_{ki}^{NAP} - H_{ji}^{laser} &= a_j + b_j U_{ji} + c_j V_{ji} \end{aligned} \quad (3-2)$$

where,

- U, V : point coordinates in a local strip frame
- a : vertical offset of the strip (GPS error)
- b, c : roll and pitch parameters
- NAP : the national height system, i.e. the reference height

Equation (3-2) can be derived as,



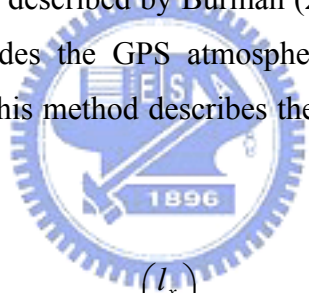
$$\begin{aligned} \begin{bmatrix} H_{ki}^{laser} - H_{ji}^{laser} \\ H_{ki}^{NAP} - H_{ji}^{laser} \end{bmatrix} + \begin{bmatrix} V_{H_{ki}^{laser} - H_{ji}^{laser}} \\ V_{H_{ki}^{NAP} - H_{ji}^{laser}} \end{bmatrix} &= \begin{bmatrix} -1 & -U_{ki} & -V_{ki} & 1 & U_{ji} & V_{ji} \\ 1 & U_{ji} & V_{ji} & & & \end{bmatrix} \begin{bmatrix} a_k \\ b_k \\ c_k \\ a_j \\ b_j \\ c_j \end{bmatrix} \quad (3-3) \\ \begin{bmatrix} H_{ki}^{NAP} - H_{ji}^{laser} \end{bmatrix} + \begin{bmatrix} V_{H_{ki}^{NAP} - H_{ji}^{laser}} \end{bmatrix} &= \begin{bmatrix} 1 & U_{ji} & V_{ji} \end{bmatrix} \begin{bmatrix} a_j \\ b_j \\ c_j \end{bmatrix} \end{aligned}$$

The observations for this equation come from ‘patches’ (used as tie ‘points’) in the ALS data. Rather than using a single point, the patches (50x50 m² areas) with many points in a flat area are used. Using patches results in a higher accuracy. This helps to reduce the random

noise associated with using a single point. The ‘tie’ points are entered into a least-squares equation and three parameters are solved for each strip. Control points, if available and observable, are also added as observations. When control is not used, the ALS data strips should be laid out and flown in a way to maximize differences between them.

An intuitive procedure would be to fly strips in opposite directions, similar to the procedure adopted in photogrammetry. One set of parameters can be solved for the entire data, but better results were found by assigning three parameters to each strip. Although the results based on this method demonstrates a reduction in overlapping errors, further analysis shows evidence of additional systematic errors. The most obvious error is the heading boresight error. The model of heading boresight error will be used to recover the systematic errors from overlapping laser strips in this research, and it is called the model of “strip adjustment with three-parameters.”

Next, a calibration method described by Burman (2000), adds the heading misalignment. This calibration method includes the GPS atmospheric errors (datum shift). Rather than solving for linear parameters, this method describes the boresight angles as a rotation matrix, i.e.



$$\begin{pmatrix} X \\ Y \\ Z \end{pmatrix}_l = \begin{pmatrix} X_0 \\ Y_0 \\ Z_0 \end{pmatrix} + \begin{pmatrix} X_d \\ Y_d \\ Z_d \end{pmatrix} + (R_{INS} \cdot R_{INS}^{LRF}) \cdot \begin{pmatrix} l_x \\ l_y \\ l_z \end{pmatrix}_{LRF} \quad (3-4)$$

where,

- $(X, Y, Z)_l^T$: the ground coordinate
- $(X_0, Y_0, Z_0)^T$: the GPS coordinate of the laser scanner
- $(X_d, Y_d, Z_d)^T$: the datum shift
- R_{INS} : the rotation matrix with attitude information from the INS
- R_{INS}^{LRF} : the misalignment between the INS and the laser head
- $(l_x, l_y, l_z)^T$: the laser components

For simplification, the following denotations are introduced:

$$R = R_{INS} \cdot R_{INS}^{LRF} \quad (3-5)$$

$$\bar{R} = R_{INS} \cdot \bar{R}_{INS}^{LRF}$$

To derive a rectangular grid of elevations, where increments are labeled as i and j , the following equation is employed

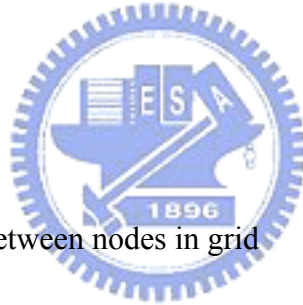
$$Z_{i,j} = f_z(X, Y) = F_Z(i, j) \quad (3-6)$$

The gradient in Z , which is a function of X and Y , is finite and exists for all Z .

$$Z'_X = \frac{\partial f_z}{\partial X} = \frac{Z_{i+1,j} - Z_{i,j}}{X_{step}} \quad (3-7)$$

$$Z'_Y = \frac{\partial f_z}{\partial Y} = \frac{Z_{i+1,j} - Z_{i,j}}{Y_{step}}$$

$(X, Y)_{step}$: the distances between nodes in grid



A laser shot, $(X, Y, Z)_l$, can be related to the grid through interpolation of the four surrounding nodes.

$$Z_l = (1-x) \cdot (1-y) \cdot Z_{i,j} + x \cdot (1-y) \cdot Z_{i+1,j} + (1-x) \cdot y \cdot Z_{i,j+1} + x \cdot y \cdot Z_{i+1,j+1} \quad (3-8)$$

$$x = \frac{(X_l - X(i))}{X_{step}}; \quad y = \frac{(Y_l - Y(i))}{Y_{step}} \quad (3-9)$$

where,

$(X, Y, Z)_l$: the laser shot coordinate

$X(i), Y(j)$: grid coordinates

x, y : the normalized position coordinates within four nodes

After linearization, the observation equation for elevation measurement (combining equation 3-4 and 3-8) becomes:

$$\lambda_{z_i} = Z'_X \cdot dX_d + Z'_Y \cdot dY_d + \left(Z'_X \frac{\partial R_X}{\partial r} + Z'_Y \frac{\partial R_Y}{\partial r} - \frac{\partial R_Z}{\partial r} \right) \cdot \begin{pmatrix} l_x \\ l_y \\ l_z \end{pmatrix} \cdot dr + \quad (3-10)$$

$$\left(Z'_X \frac{\partial R_X}{\partial p} + Z'_Y \frac{\partial R_Y}{\partial p} - \frac{\partial R_Z}{\partial p} \right) \cdot \begin{pmatrix} l_x \\ l_y \\ l_z \end{pmatrix} \cdot dp + \left(Z'_X \frac{\partial R_X}{\partial h} + Z'_Y \frac{\partial R_Y}{\partial h} - \frac{\partial R_Z}{\partial h} \right) \cdot \begin{pmatrix} l_x \\ l_y \\ l_z \end{pmatrix} \cdot dh +$$

$$(1 - \bar{x}) \cdot (1 - \bar{y}) \cdot Z_{i,j} + \bar{x} \cdot (1 - \bar{y}) \cdot Z_{i+1,j} + (1 - \bar{x}) \cdot \bar{y} \cdot Z_{i,j+1} + \bar{x} \cdot \bar{y} \cdot Z_{i+1,j+1}$$

where,

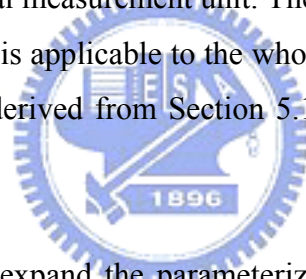
z_i	: discrepancy between measured and approximate value
(dX_d, dY_d, dZ_d)	: updates to the unknown datum shift
r, p, h	: roll, pitch, heading
dr, dp, dh	: updates to the unknown misalignment angles
$dZ_{i,j}$: updates to the unknown elevation grid
\bar{x}, \bar{y}	: approximate values of normalized coordinates within the four surrounding grid points

This method can be implemented with or without ground control. Without ground control the datum error cannot be determined - it is therefore assumed to be zero. Unlike the previous method, which requires leveled surfaces, this method exploits sloped surfaces to determine misalignment. With sloped surfaces, larger differences can be seen in overlapping strips. Points of interest for tie points were found by passing a Sobel edge detector over the rasterized height image. It was found, however, that vegetation and irregular structures on the surface interfered with automated point extraction. Manual intervention was required to obtain suitable observation points.

The corresponding points were then found in the other strips and the observations are added to a least-squares equation. One set of misalignment angles is then solved for the entire data set. Analysis of the results still indicated further sources of error, however. In addressing the sources of error associated with this method, a commercial strip adjustment software, *TerraMatch* (Burman, 2002; Burman & Soininen, 2004), is then developed by *TerraSolid Inc.*

The *TerraMatch* software is designed to model systematic orientation errors in ALS data. It measures the differences between laser surfaces from overlapping, flight-lines or differences between laser surfaces and known points. These observed differences are translated into correction values for system orientation – easting, northing, elevation, heading, roll and pitch (Burman and Soininen, 2004).

TerraMatch can be used as a laser scanner calibration tool or as a tool for improving actual project data. When used as a calibration tool, it will solve the misalignment between the laser scanner and the inertial measurement unit. The end result is a set of correction values for heading, roll and pitch that is applicable to the whole data set. To evaluate the accuracy of the misalignment parameters derived from Section 5.1, the *TerraMatch* is used to solve the misalignment parameters.



Next, two other methods expand the parameterization to include IMU drift rates. This method presented by Behan et al. (2000), like the Crombaghs et al. (2000) method, also solves for parameters on a strip-by-strip basis. Unlike Crombaghs et al. (2000), however, the Behan et al. (2000) model is based on the general ALS target Equation (3-11). This method employs tie points from the strips in a local strip coordinate frame (Figure 3.1).

$$\begin{pmatrix} X \\ Y \\ Z \end{pmatrix} = R_{strip_to_ref} \cdot (R_e + x R_{et}) \begin{bmatrix} x \\ y \\ z \end{bmatrix} + \begin{pmatrix} e_x \\ e_y \\ e_z \end{pmatrix} + \begin{pmatrix} X_{stripcenter} \\ Y_{stripcenter} \\ Z_{stripcenter} \end{pmatrix} \quad (3-11)$$

$$\text{with } R_e = \begin{pmatrix} 1 & -\kappa & \varphi \\ \kappa & 1 & -\omega \\ -\varphi & \omega & 1 \end{pmatrix} \text{ and } R_{et} = \begin{pmatrix} 0 & \dot{\kappa} & \dot{\varphi} \\ \dot{\kappa} & 0 & -\dot{\omega} \\ -\dot{\varphi} & \dot{\omega} & 0 \end{pmatrix}$$

- $(X, Y, Z)^T$: the reference coordinate system
 $(x, y, z)^T$: the ideal (error free) strip coordinate system
 $R_{strip_to_ref}, X_{stripcenter}, Y_{stripcenter}, Z_{stripcenter}$: the transformation between the reference system and ideal strip system
 $(e_x, e_y, e_z)^T$: the three offsets
 $(\omega, \varphi, \kappa)$: the three rotations
 $(\dot{\omega}, \dot{\varphi}, \dot{\kappa})$: the time-dependent rotations

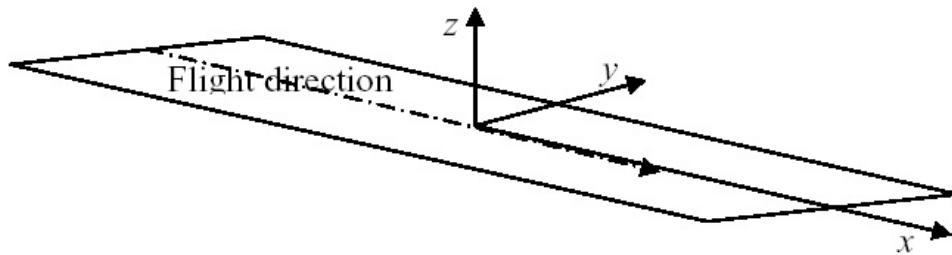


Figure 3. 1: Strip coordinate frame

In the strip frame, the positive X axis corresponds to the platform's line of flight. In this way, the time-dependent parameters of IMU drift can be replaced by U, which is the x coordinate of a point in the strip frame that correlates with time. This method requires ground control points within the mission area to solve for all 9 parameters per strip. Behan et al. (2000) attempted to implement an automated tie point extraction algorithm by searching for gradients in the elevation data. Due to problems associated with occlusion and resolution, however, they resorted to manual observations. Their results showed the greatest reduction in residual error, compared to the other methods presented in this section. However, because they solved for parameters on a strip basis, this method is not truly a calibration of systematic errors, but rather a post-mission polynomial adjustment.

Filin (2001 & 2003) presented an error recovery model based on modeling the system errors in laser altimetry and defining adequate control information. Instead of finding corresponding points, the idea of corresponding surface is proposed. Filin (2001) utilized natural and man-made surfaces to recover the calibration parameters. These surfaces are quite general. This model is tested for finding two main error sources in the ALS system, namely,

the mounting and the range bias. By analyzing the properties of the proposed method, it has been demonstrated that moderate slopes are sufficient to generate reliable solutions (Filin, 2001 and 2003).

$$s \begin{bmatrix} X_0 \\ Y_0 \\ Z_0 \end{bmatrix} + R_{INS} \left(\begin{bmatrix} \delta_x \\ \delta_y \\ \delta_z \end{bmatrix} + R_m R_s \begin{bmatrix} 0 \\ 0 \\ -(\rho + \delta\rho) \end{bmatrix} \right) + s \begin{bmatrix} \bar{e}_x \\ \bar{e}_y \\ \bar{e}_z \end{bmatrix} + s_4 = 0 \quad (3-12)$$

Morin (2002) and Morin and El-sheimy (2002.) developed and implemented a new calibration method for an ALS. The authors addressed the shortcomings in current manual methods by eliminating a need for ground control points, providing a rigorous stochastic model, modeling additional sources of error, and improving the speed of an ALS calibration. The details of the proposed method will be described in Section 4.1.

Lee et al. (2003) proposed a least-squares adjustment to reduce the horizontal error of ALS data. This method adjusts for the error that is introduced mainly by the drift of the IMU, causing systematic differences between strips on the same area. The mathematical model is largely based on Kilian et al. (1996) model. To effectively capture the tie points, Lee et al. (2003) developed a set of procedures that construct a DSM with break lines and then performed feature-based matching on strips, resulting in a set of reliable tie points. The ground control points are manually selected to ensure that all points are present on maps on the scale of 1:1,000. Solving the observation equations by the least-squares method produces a set of affine transformation equations with 6 parameters, which are used to transform the strips for adjusting the horizontal error.

Applying a similarity transformation, Csanyi and Toth (2004) and Csanyi et al. (2005) used a well-identified, LiDAR-specific ground targets (Figure 3.2) to adjust the ALS data. The proposed ground targets are used as GCPs in the adjustment process. The test results showed that the specifically designed ALS targets are indeed useful in improving the accuracy of road surface extraction and other applications that require engineering scale mapping accuracy.



Figure 3.2: Ground control target for ALS (Csanyi, 2005)

Further work in strip adjustment of ALS data can be found in Elberink et al. (2003), Kornus and Ruiz (2003), and Kager (2004).

3.1.2 Accuracy assessment

Accuracy of the ALS data becomes an important issue as the number of LiDAR applications and commercial LiDAR data vendor increases.

Huising and Pereira (1998) estimated the errors and accuracy of ALS data derived from 5 different ALS systems. The errors of ALS systems were categorized as laser ranger induced error, navigation system induced error, filtering error, and others. Their study shows that errors related to the laser instrument, namely GPS and INS, may frequently occur, resulting in local distortions, and planimetric and height shifts. This work contributed to the design of appropriate strategies for data collecting and processing in earlier stages of ALS systems.

A pure statistical method for estimating the relative LiDAR accuracy by comparing overlapping LiDAR datasets is described in Latypov (2002). This method begins with the definition of a relative accuracy estimate, which is generalized from a measure of point-to-point closeness to a measure of surface-to-surface closeness. A problem of matching the

individual point in the overlapping datasets is eliminated. The generalized accuracy estimate is a function of surface size and flatness (equation 3-6). Sampling overlap area by surfaces of different size allows one to discriminate between the random, systematic and locally systematic errors. The relative accuracy in the traditional sense of using only some tie points is a limited case of the generalized one and can also be computed.

$$f = \frac{1}{A} \int_{As} \sqrt{(\partial g / \partial x)^2 + (\partial g / \partial y)^2} dx dy \quad (3-13)$$

where,

g : gradient

A : area (size) of As

Maas (2000, 2001, & 2002) proposed the least-squares matching on the height data in a TIN (triangulated irregular network) data structure to avoid a loss of information due to grid of the height data. Points near height jump edge were excluded from the matching by eliminating the triangles with a steep slope. The DSM (digital surface model) of one strip is considered as the reference. The distances between the points of the other strip and the DSM are to be minimized.

The corresponding positions between strips are estimated by using the height data for the determination of the Z-discrepancies, and the reflectance (intensity) data for the determination of the planimetric discrepancies. Furthermore, points falling into occlusion zones, which are characterized by TIN-meshes with irregular shape and size, have to be excluded from the matching process to avoid the occlusion (Figure 3.3). When the matching is applied to practical tests, the precision potential for the planimetric shift parameters reaches decimeter-level, and is estimated to be on the order of 1/10 to 1/20 of the average point spacing. This method provides good matching of points, but automatically determining a feature from elevation data alone was still problematic.

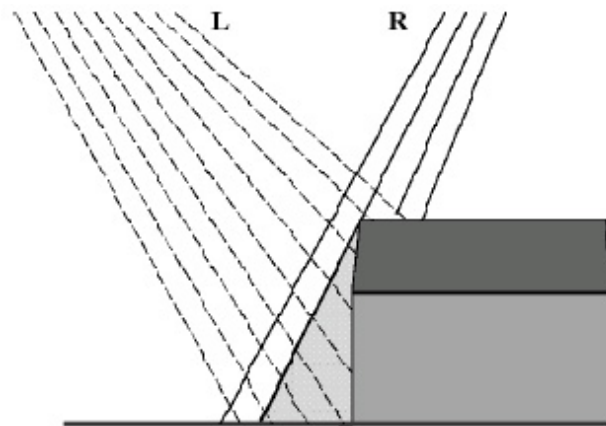


Figure 3.3: Occlusion in the right strip at a building

The registration of data sets in the same coordinate system is an essential task in the fusion of data acquired from similar or different sources. The surface matching algorithms may be expected to become an important tool of data fusion, especially with data acquisition techniques such as ALS that lack thematic information. Paquet (2003) demonstrated that the accuracy of the registration, both in height and plan positioning, as well as the accuracy of the matching, is related to the density of the reference data based on the proposed least-squares surface matching.

A cross-validation method is used to find the accuracy of the registration and the mean of the matching residuals for different densities of the reference surface. The artificial data and practical ALS data are used in this study. This study shows that the curves generated by a cross-validation method can be modeled on hyperbolic functions. The hyperbolic functions are used to predict accuracy for densities that are higher than those used for the validation. The accuracy of the predictions reached sub-millimeter level. The accuracy of the registration of the ALS data ranged from millimeter to decimeter. The accuracy is improved with the increase of ALS data density.

Hodgson and Bresnahan (2004) conducted the accuracy of airborne LiDAR-derived elevation based on empirical assessment of error budget. The horizontal coordinates of LiDAR points were located in the field and these elevations were surveyed, rather than using an interpolation approach for gathering observed elevations at reference points. The variability of height accuracy was evaluated for 6 land-cover categories. An error budget

model was then created for the observed LiDAR elevation error. The observed error was decomposed into several types including errors from LiDAR system measurement, errors from horizontal displacement, interpolation error, and surveyor error. A cross-validation approach was used to assess the observed interpolated LiDAR elevation error for each field-verified reference point.

Next, Ahokas et al. (2004) presented a quality assessment of ALS data on height as well as planimetric accuracy. The ground reference points are used to check the height discrepancies, and the centers of buildings and ridges are applied to evaluate the planimetric offsets. It can be concluded that the change in height errors of five dense ALS strips are negligible. The planimetric accuracy of the building on the ground depends on the direction of the flight. Furthermore, the accuracy obtained using the center points of the buildings depends on the extraction accuracy and the distribution of the laser points on the ground.

Other studies regarding the ALS data accuracy assessment, include Lohmann and Koch (1999), Casella and Spalla (2000), Behan (2000), Schenk et al. (2001a), Casella (2003), Artuso et al. (2003), Alharthy et al. (2004), Ronnholm (2004), etc.

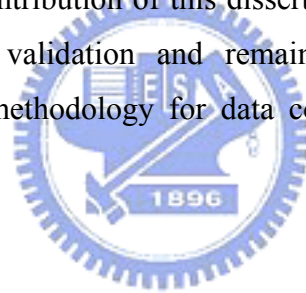
3.2 The contribution of this research

The background (Chapter 2) and literature review in the preceding section reveals that the research on calibration, systematic error validation, and data adjustment on ALS data are far from complete. For calibration of ALS system, on the one hand, the adaptation of photogrammetric concepts is not always appropriate. A solution that originates from an analysis of the data acquisition model is therefore needed. On the other hand, correspondence problems also need to be worked out, regardless of the models applied. These problems motivate this dissertation to evaluate one of the calibration solutions proposed by a commercial ALS vendor. This solution introduces the reflectance intensity of laser to measure corresponding points, i.e. tie points. The objective of the first part of the evaluation is to find an efficient method to improve the tie point measurement. The evaluation of improvement is based on the control information.

Next, systematic error validation, which is the second part of the evaluation, is motivated to examine how to validate ALS data by consistent checks, particularly for a user who obtains calibrated ALS data from data suppliers. Systematic error validation is involved to check the accuracy with the calibrated data derived from the first part of the evaluation. The proposed method on systematic error validation works solely without control information. Furthermore, an efficient solution for establishing the correspondence between overlapping strips is presented.

In addition, prior work on systematic error validation reveals that the remaining systematic error may result in lower accuracy after the ALS calibration. Due to a shortage of ground truth, a different view of the registration of laser data is proposed to reduce the remaining systematic errors based on the similarity transformation and the three-parameter strip adjustment.

In summary, the major contribution of this dissertation presented a complete scheme on calibration, systematic error validation and remaining systematic error recovery. The proposed scheme offers the methodology for data correction as well as a quality control mechanism for ALS data.



CHAPTER 4

METHODOLOGY

4.1 ALS boresight calibration

The problems involving calibration has been discussed in Chapter 2. The first part of this chapter is to evaluate a calibration method which is currently used by the Leica ALS system. This method is based on Morin's (2002) work. The mathematical model and flight planning are described first, followed by the improvement and analysis of this method.

The process to recover all the systematic errors discussed in Section 2.2 is a very complicated task. Therefore, this research only focuses on boresight calibration, that is, boresight misalignment angles (roll, pitch and heading), torsion error and elevation offset.

4.1.1 Mathematical model

The calibration model begins with a simple observation equation:

$$r_i^m = r_{nav}^m(t) + R_b^m(t) [R_S^b \cdot r_i^S + a^b] \quad (4-1)$$

where:

- r_i^m : coordinate of laser target (i) in the mapping frame (m-frame)
- $r_{nav}^m(t)$: coordinate of the combined navigation sensors (GPS/IMU) in the mapping frame
- $R_b^m(t)$: the interpolated rotation matrix from the navigation body frame(b-frame) to the mapping frame

- R_s^b : rotation from body frame to the scanner frame (s-frame) to the body frame, i.e. the boresight misalignment angles
 r_i^S : laser vector from scanner in s-frame
 a^b : coordinate offset between the b-frame and the s-frame

The laser components are expanded to include the scanner angle:

$$r^s = R_L^S(t) \cdot r^L = R_L^S(t) \cdot \begin{pmatrix} 0 \\ 0 \\ d \end{pmatrix}^L \quad (4-2)$$

where:

- $R_L^S(t)$: the rotation from the laser frame to the scanner frame using the scanner mirror angle β
 r^L : the laser range vector in the laser mirror frame(L-frame)
 d : the corrected range measurement from the laser

Combined, the sensor equation becomes:

$$r_i^m = r_{nav}^m(t) + R_b^m(t) [R_s^b \cdot R_L^S(t) \cdot r^L + a^b] \quad (4-3)$$

where:

- $R_b^m(t)$: a full rotation matrix with roll, pitch and heading taken from the navigation sensor (Ω, Φ, K)
 R_s^b : a full rotation matrix of the misalignment parameters (ω, ϕ, k)
 $R_L^S(t)$: a rotation matrix about the secondary axis with the scanner angle (β)

The equation is the base model from which additional parameters can be added. To add a parameter for the scanner error due to torsion, the scanner angle must be expanded:

$$\beta = \beta_0 + \delta + \varphi \quad (4-4)$$

where:

- β : the corrected scan angle used in the scanner rotation matrix $R_L^S(t)$
- β_0 : the raw scanner angle from the scan angle encoder
- δ : the sum of the scanner corrections
- φ : the atmospheric correction

The scanner corrections for torsion can be modeled as a function of the raw scanner angle, i.e.:

$$\delta_{torsion} = c \cdot \beta_0 \quad (4-5)$$

where:

- c : a constant correction value for torsion

The combined equation for each epoch is then:

$$r^m = r_{nav}^m + R_b^m\{\Omega, \Phi, K\} [R_s^b\{\omega, \phi, k\} \cdot R_L^S\{\beta, c\} \cdot r_i^L + a^b] \quad (4-6)$$

The unknown calibration parameters for this equation are:

$$\bar{x} = [\omega, \phi, k, c] \quad (4-7)$$

The unknown parameters can be solved by observing control points in the ALS data. The use of control points allows a parametric least-square model to be formed, and a unique solution to the calibration parameters can be found. It is highly desirable, however, to implement a calibration method that does not rely on known ground control points (Morin, 2002).

One way to solve the observation equation is to observe distinct features in the overlapping area. These features could be similar to those used in conventional photogrammetry such as road markings; but should avoid non-continuous features such as building edges due to the increased possibility of mismatching. The criteria to select tie point are described in Section 4.1.3. The calibration errors result in coordinate discrepancies

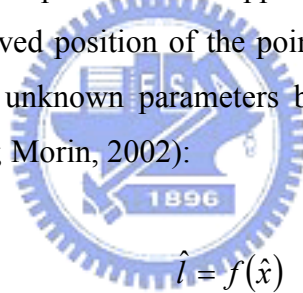
between the common features. A calibration solution can therefore be found by minimizing these discrepancies, i.e. for a feature observed in 4 overlapping strips:

$(X, Y, Z)_{target}^i$: A user observes the feature in each strip,

If the effects of the calibration errors are uncorrelated in the feature observations, then the average of the feature coordinates should be approximately the value of the true position,

$$\begin{pmatrix} \bar{X} \\ \bar{Y} \\ \bar{Z} \end{pmatrix}_{average} = \frac{1}{n} \sum_{i=1}^n \begin{pmatrix} X \\ Y \\ Z \end{pmatrix}_{target}^i \cong \begin{pmatrix} X \\ Y \\ Z \end{pmatrix}_{true} \quad (4-8)$$

More details of the observation equation, which is proposed to solve the calibration parameters in this research, are presented in Appendix A. The discrepancy between the average position and the observed position of the point becomes the disclosure information, which is needed to solve the unknown parameters by least-squares adjustment, using the parametric form (Hwang, 2001; Morin, 2002):



$$\hat{l} = f(\hat{x}) \quad (4-9)$$

$$\hat{r} = A\hat{\delta} + w \quad (4-10)$$

$$w = f(x^0) - l \quad (4-11)$$

$$\hat{\delta} = (A^T C_l^{-1} A)^{-1} \cdot A^T C_l^{-1} w, \hat{x} = x^0 + \hat{\delta} \quad (4-12)$$

where:

- \hat{l} : the vector of a adjusted observations
- \hat{x} : the vector of unknowns (4-7)
- $f(\hat{x})$: the observation equations (4-6)
- \hat{r} : the vector of observation residuals to be minimized
- A : the matrix of partial derivates with respect to x
- $\hat{\delta}$: the vector of corrections to the unknowns

- w : the vector of disclosure
 x^0 : the vector of initial approximations
 l : the vector of average tie point values (4-8)
 C_l^{-1} : the prior weight matrix

In a non-linear model, this procedure must be iterated until a solution is converged to, i.e.:

$$w^{n+1} = f(x^n + \hat{\delta}^n) - l, \text{ until } \hat{\delta}^{n+1} \cong 0. \quad (4-13)$$

4.1.2 Flight planning and data collection

The discrepancies between the ALS overlapping strips should reach an apex in solving the calibration parameters with the greatest accuracy and stability. Flight planning needs to be carried out while taking into consideration the effects of calibration parameters on the resulting data. In general commercial ALS operation, calibration flights are usually flown over airports and runways, which by nature is flat. The flatness of the terrain needs to be taken into account for calibration flight while modeling the misalignment errors effects. Furthermore, some distinct features, such as road markings or intersections, should be selected as tie points if the intensity data are used.

The boresight calibration parameters, namely roll, pitch, heading, torsion and the elevation offset, are described in Section 2.2. A practical example demonstrating how to determine each boresight angle is presented in Section 2.3. The factors considered in deciding the calibration parameter include flight design, the sequence of correction, the selection of area of interest, the measurement of discrepancies and the validation.

First, roll misalignment causes the measured distance to register an incorrect location (Figure 4.1a). The effect on the registered over flat terrain is that it appears to be lower and pushed out from the center of the strip. The largest difference in overlapping strips would be created by a strip flown in the opposite direction (Figure 4.1b). Second, the same argument for the pitch misalignment error can be determined over sloped terrain. Over flat terrain, however, the height offset of a point will be very small from the two strips flown in opposite

directions. Instead, an elevation difference can be generated by flying strips at different altitudes (Figure 4.2a). A height discrepancy will then be produced (Figure 4.2b).

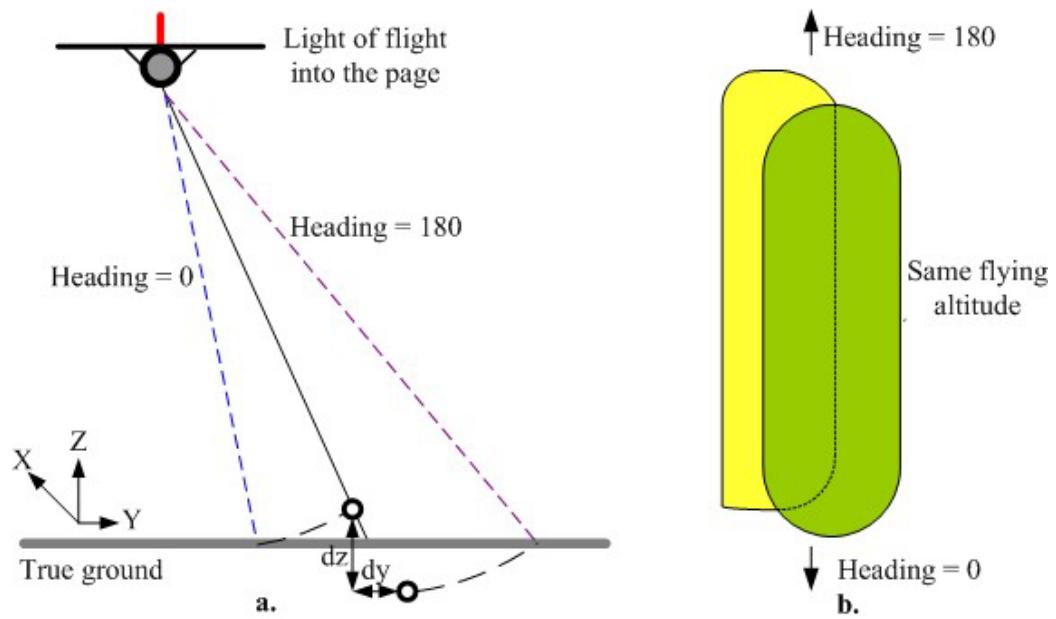


Figure 4.1: Effects of roll error on overlapping data

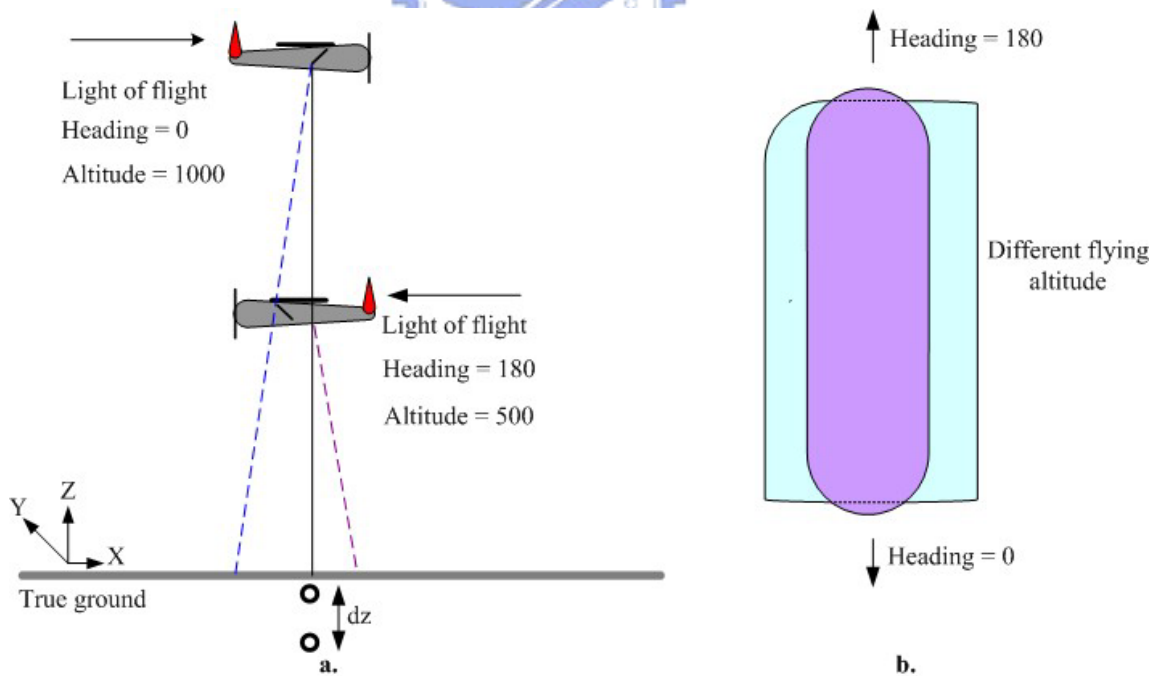


Figure 4.2: Effects of pitch error on overlapping data

Next, the heading misalignment error is the most problematic to model from tie points. If flight strips are flown in opposite directions, the forward and reverse misalignment effect will create the same displacement on the registered point (Figure 4.3a). Instead of flying in opposite directions, flight lines should be flown at 90 degrees from each other in order to maximize the discrepancies. Planimetric features are more difficult to measure accurately, however, due to the lower horizontal accuracy of ALS data. This can be observed in the variance of the heading solution.

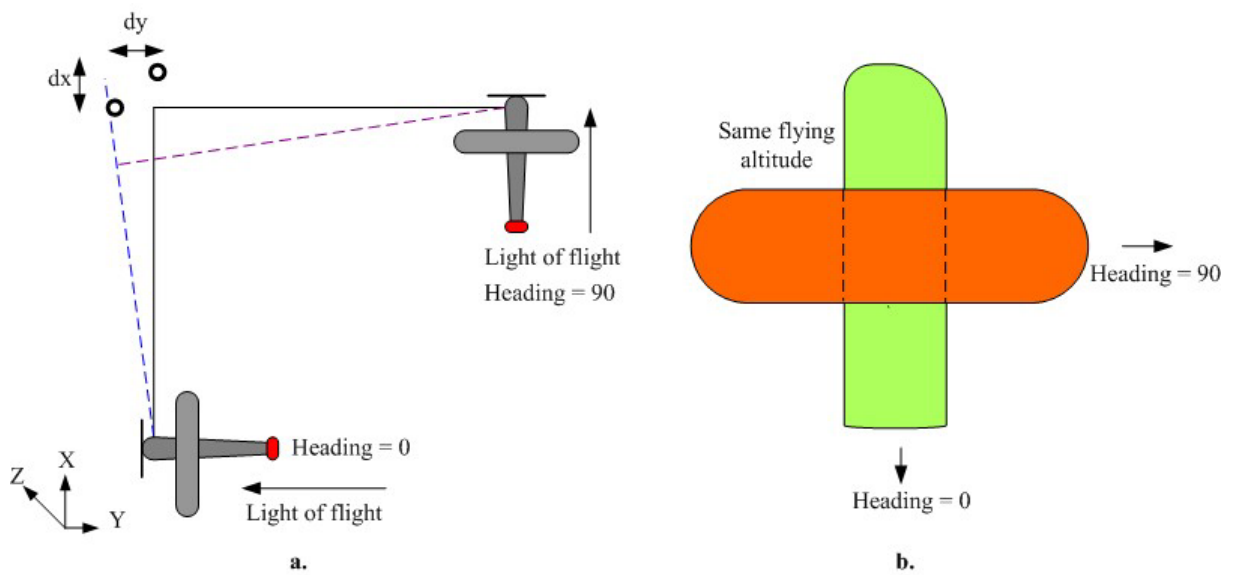


Figure 4.3: Effects of heading error on overlapping data

The last misaligned parameter, the torsion, inducing the bowing in the ALS data strip is also symmetric. It cannot be modeled by a simple flight line in an opposite direction. The elevation differences from torsion errors will increase with altitude and scan rates. To observe the differences, flight lines should be arranged so that the edges of the strips (the ones that have the most torsion error) overlap with the center of the strips with minimal torsion error (Morin, 2002). Similar to the heading error, the differences are maximized by flying at 90 degrees. The torsion error will create height offsets, however, which permit that parameter to be determined more accurately. An optimal ALS calibration flight pattern can be derived as shown in Figure 4.4 while integrating the different requirements for each parameter (Burman, 2000a; Morin & El-Sheimy, 2002; Leica, 2003a).

The calibration method described above does not require control points to determine the 3-boresight angles and the torsion value. However, there is at least 1 known ground control point (GCP) needed to determine a Z offset (elevation offset). The control point does not need to be signalized. They can be placed anywhere in the observation area (Leica, 2003a). Once the ALS flight lines have been corrected for the misalignment, the control points are simply differenced with the elevation in the strip.

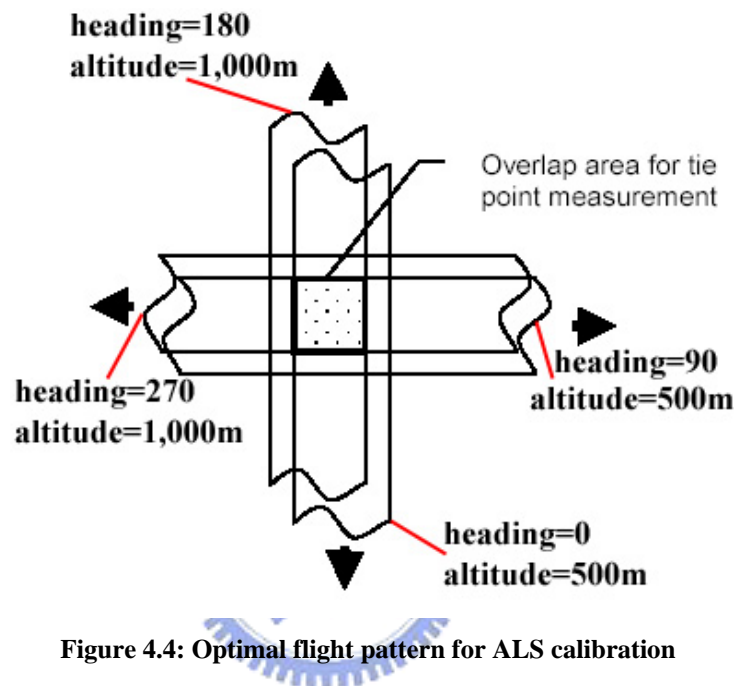


Figure 4.4: Optimal flight pattern for ALS calibration

Once a suitable dataset following the calibration flight (Figure 4.4) has been obtained, tie points can be observed in the overlapping areas within the strips. The non-continuous nature of the ALS data presents another challenge. As was discussed, it is highly unlikely that laser pulses from different strips will strike a feature in the same way. The ALS points have to be interpolated in order to identify the position of a common feature from the laser data. The interpolated grid is then used to measure tie points.

4.1.3 Attune program

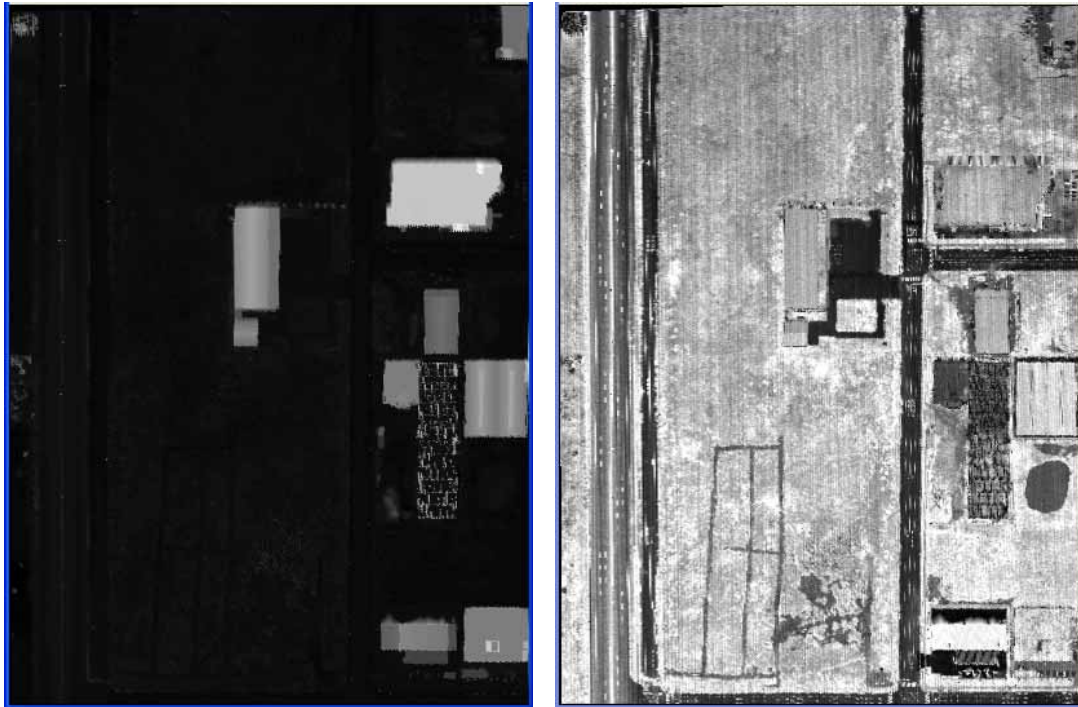
Most LiDAR systems nowadays have the possibility of recording the intensity of the reflected laser pulse (Vosselman, 2002a; Maas, 2002). This reflectance value is sometimes used for visualization purposes or in segmentation tasks (Maas, 2000). The intensity of ALS

is defined as the ratio between the magnitude of received light and emitted light. The intensity of ALS is influenced mainly by the reflectance value (reflectivity) of the reflecting object (Song, et al., 2004). Reflectance varies with material characteristics as well as the light used. Different materials have different reflectance values. Many materials have a fairly low reflectance value.

A laser signal detector is usually configured to anticipate a weak return signal. Some materials such as the retro reflective pad, however, have very high reflectivity. The power of the returned signal is very high and can saturate a laser detector that anticipates weak return signals. The effect on the ground points is usually manifested by very bright points appearing to 'hover' above the surrounding terrain. Some commercial systems implement an automatic gain control (AGC) to compensate for the returned signal. Therefore, the AGC attempts to normalize the return intensity so that low signals are dropped out and false ranges from saturated signals are reduced (Leica, 2004b; Hentschel, 2005).

Several researchers suggested or proposed methodologies to use the intensity data for the estimation of planimetric offsets between airborne laser scanning strips (Burman, 2000a; Maas, 2002). Song et al. (2002) evaluated the suitability of ALS intensity data for land-cover classification. Song et al. (2002) suggested that the ALS intensity data need to be normalized by the angle of reflection to decrease the noise.

The intensity data often contain much more detailed information than what can be used to determine offsets (Vosselman, 2002a; Maas 2002). As Figure 4.5 shows, the ground features with minor terrain variation are difficult to discern in the visualized height data (Figure 4.5a). In contrast, roads, road marking, trail path, etc. can be easily identified using the ALS intensity reflectance data (Figure 4.5b).



a. Height data

b. Intensity data

Figure 4.5: Comparison of height and intensity data of ALS

The program for calibrating ALS system in this study utilizes the intensity data to select the tie points. The *Attune* program is designed to calibrate *Leica Geosystems ALS* series ALS instrument (Leica, 2003a) based on Morin's work (Morin, 2002). The primary calibration parameter determined by the user is mechanical misalignment between the IMU and the receiving optics in the scanner. The misalignment is described by a roll, pitch, and heading error (i.e. the boresight angles). The procedure involves mathematically modeling the torsion of the rotating mirror and the angular misalignment. This parameter affects the results due to the combined dynamics of the rotating mirror and the angular alignment, as was discussed in Section 2.2.1. Finally, a Z shift, which calibrates the instrument vertically to a known datum, is determined.

With this program, the user identifies common features that are visible in the ALS intensity images. The initial differences between these tie points are minimized to determine the calibration parameters based on the mathematical model in Section 4.4.1.

The tasks of *Attune* software involves organizing files, generating images, providing interface for selecting tie points, and performing calibration parameter refinement. This program is integrated with other softwares to complete the calibration procedures, including *Leica ALS Post Processor* (Leica, 2004b), *Bentley MicroStation*, and *TerroSolid TerraScan*.

A grayscale image similar to an ortho-rectified image is generated using the intensity reflectance data from the ALS system. To this end, the intensity values of the randomly distributed point clouds are interpolated onto a regular grid spacing. The criterion used to select grid size is the average ground space of laser point clouds. As Figure 4.6 shows, this flight line is one of the ALS calibration flight lines captured from a calibration site. In order to model the differences between the strips, common features, i.e. tie points, must be identified. The points were recorded in the image coordinate (in pixels), and later converted back to mapping coordinates using the affine relationship established by the ortho-image (Morin, 2002; Leica, 2003a).

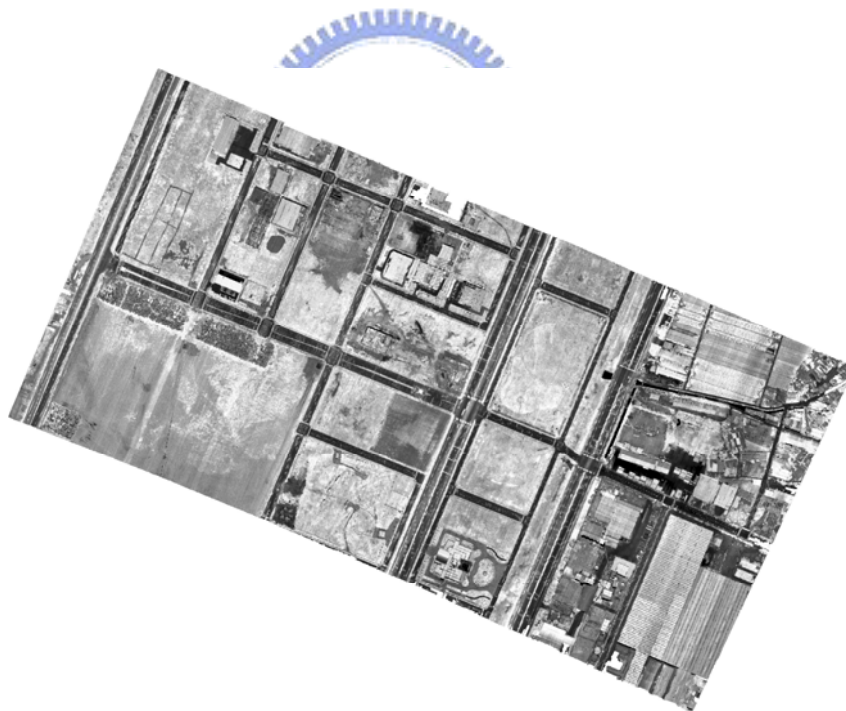


Figure 4.6: A generated grayscale image from ALS intensity data

The most critical and time-consuming operation is the tie points measurement. The quality of the measurements will affect the accuracy of the derived calibration parameters. The criteria for tie point selection are:



Figure 4.7: Road markings are selected as tie points

- Make sure the selected points appear on at least 2 images,
- Choose a distinctive feature such as a road marking or intersection (Figure 4.7),
- Avoid sharp edges such as the side of buildings or cliffs,
- Prefer local flat areas such as roads or a flat field,
- Choose 20-30 points for each image and verify that some of them can appear on all images,
- Points should spread throughout each image as much as possible, and
- Take extra measurement at the edges of the FOV. This is where the terrain displacements will be the largest.

4.1.4 Improvement on tie point selection

The motivation to improve the tie point selection is to reduce the amount of time spent on identifying the common features on each image with the software *Attune*. Furthermore, the grayscale image generated from ALS intensity data is much different from the regular images taken with optical cameras. A key issue under investigation in this research is whether it is

possible to apply image matching techniques to identify the tie points instead of measuring the tie points manually.

In Morin (2002), the *Interactive Point Measurement (IPM)* tool in *Leica Geosystems SOCET SET* was used to collect tie points in overlapping images based on auto-correlation techniques. The operation of common-feature selection is very similar to the automatic tie point generation in existing soft-copy photogrammetry workflows. However, the results were very poor. Morin (2002) concluded that the low resolution, coupled by the varying response of the intensity information based on the angle of incidence, did not permit autocorrelation techniques to work as well as they might in a standard photogrammetry problem.

Behan (2000) used the Forstner interest operator (Forstner, 1986; Luhmann and Altrogge 1986) to obtain candidate points for matching in order to derive the tie points. He also performed least-squares matching for neighboring cells. The results were not sufficiently satisfactory. Behan (2000) then selected the matching points manually instead. He attributed the unsatisfactory results to erroneous distortions that occurred during interpolation in rasterization of the irregularly-spaced raw data. In contrast, Maas (2000, 2002) have shown that a significant improvement in the quality of matching results is possible using least-squares matching directly on a TIN of laser points.

An image matching method is proposed in this study to identify the tie points with some improvements. First, the ALS strips data are pre-processed via the suggested procedures in Section 4.4 to decrease the memory requirement. Second, the overlapping areas in all strips will be divided into some patches – for this study, 6 patches. The differences between corresponding patches for each two strips will therefore be smaller than the whole image. Next, choose the specific image generated from ALS intensity data for an interest point detector.

In Schmid et al. (2000), two novel criteria are used to evaluate interest points: repeatability and information content. These two criteria directly measure the quality of the feature for tasks like image matching, object recognition, and 3-D reconstruction. Repeatability explicitly compares the geometrical stability of the detected interest points

between different images of a given scene taken under varying viewing conditions. Information content is a measure of the distinctiveness of an interest point. Distinctiveness is based on the likelihood of a local grayscale descriptor computation at the point within the population of all observed interest point descriptors. The entropy of these descriptors measures the information content of a set of interest point (Schmid et al, 2000). There are five interest point detectors evaluated in this study, including Harris, Forstner, Cottier, Heitger, and Horaud. Schmid et al. (2000) concluded that Harris interest point detector is better than or equivalent to those of other detectors across different conditions on the repeatability criteria. The results for information content again show that the Harris interest point detector obtains the best results.

The conclusions of Schmid et al. (2000) and Dufournaud et al. (2004) lead this research to select Harris detector (Harris and Stephens, 1988) as the interest point operator. Consider the following matrix

$$M = \begin{bmatrix} \left(\frac{\partial I}{\partial x}\right)^2 & \left(\frac{\partial I}{\partial x}\right)\left(\frac{\partial I}{\partial y}\right) \\ \left(\frac{\partial I}{\partial x}\right)\left(\frac{\partial I}{\partial y}\right) & \left(\frac{\partial I}{\partial y}\right)^2 \end{bmatrix} \quad (4-14)$$


where $I(x,y)$ is the gray level intensity. If at a certain point the two eigen values of the matrix M are large, then a small motion in any direction will cause a significant change of gray level. This indicates that the point is an interest point. The interest point response function is given by:

$$R = \det M - k(\text{trace}M)^2 \quad (4-15)$$

where k is a parameter set to 0.04 (as Harris suggested). Interest points are defined as local maxima of the interest response function. To avoid interest points caused by image noise, it may be advantageous to smooth the images with a Gaussian filter. This should, however, not

be done on the original input images, but on images containing the squared image derivatives (that is $(\frac{\partial I}{\partial x})^2, (\frac{\partial I}{\partial y})^2, (\frac{\partial I}{\partial x}), (\frac{\partial I}{\partial y})$).

Next, an area-based matching technique is used in this study. The area-based matching, also called signal-based matching, is associated with image gray levels. That is, the gray level distribution of small areas of two images is compared and measured for similarity. Similarity measure is a quantitative measure of how well matching entities correspond to each other. Generally, the degree of similarity is measured by the cross-correlation coefficient (equation 4-16) or the standard deviation in least-squares matching (Schenk, 1999; Kropatsch and Bischof, 2001). One of the images is chosen to be the reference image (the template), its gray levels will be denoted by g_1 ; the other image will be called search image and its gray levels denoted by g_2 .

$$\rho = \frac{\sum_{r=1}^R \sum_{c=1}^C (g_1(r,c) - \mu_1)(g_2(r,c) - \mu_2)}{\sqrt{\sum_{r=1}^R \sum_{c=1}^C (g_1(r,c) - \mu_1)^2 (g_2(r,c) - \mu_2)^2}}; -1 \leq \rho \leq 1 \quad (4-16)$$

where,

- $g1(r,c)$: individual gray values of template matrix
- $\mu 1$: average gray value of template matrix
- $g2(r,c)$: individual gray values of corresponding part of search matrix
- $\mu 2$: average gray value of corresponding part of search matrix
- R, C : number of rows and columns of template matrix

Both height and intensity data are applied to detect the tie points by using the proposed image matching technique. Affirmatively, there will be incorrectly-matched pairs. A method employed to remove the incorrectly-matched pairs in this study is based on a non-iterative scheme (Hsieh et al., 1997). The removal method is based on the idea that the distance between two points in the same image will be preserved when it undergoes a rigid transformation. Let $MP = \{p_i \leftrightarrow q_i\}_{i=1,2,\dots,N_m}$ be a set of matching pairs, where N_m represents the

number of matched pairs in MP , $p_i = (p_x^i, p_y^i)^t$ is a point in $f_1(x, y)$, and $q_i = (q_x^i, q_y^i)^t$ is a point in $f_2(x, y)$. If all the matching pairs in MP are correct, then the following equation should hold, that is,

$$p_i = sq_i + T \quad \text{for } i = 1, 2, \dots, N_m, \quad (4-17)$$

where s and T are, respectively, a scalar and a translation vector. Let $\{p_i \Leftrightarrow q_i\}$ and $\{p_j \Leftrightarrow q_j\}$ be two correct matching pairs in MP . The scale s between $f_1(x, y)$ and $f_2(x, y)$ can be estimated as

$$s = d_2/d_1 \quad (4-18)$$

with $d_1 = \sqrt{(p_x^i - p_x^j)^2 + (p_y^i - p_y^j)^2}$ and $d_2 = \sqrt{(q_x^i - q_x^j)^2 + (q_y^i - q_y^j)^2}$. The translation T_i between p_i and q_i can be calculated by using equation 4-17 when scale s is computed. Moreover, the translation T_j between p_j and q_j can be obtained accordingly. Since the pairs $\{p_i \Leftrightarrow q_i\}$ and $\{p_j \Leftrightarrow q_j\}$ are correctly-matched pairs, the difference between T_i and T_j should be very small. Therefore, by checking the distance between T_i and T_j , we can determine whether $\{p_i \Leftrightarrow q_i\}$ and $\{p_j \Leftrightarrow q_j\}$ are correctly-matched. More details about the algorithm to remove the incorrectly-matched pairs are described in Hsieh et al. (1997) and Chen (2000).

The work flow regarding the improvement of the tie point selection is depicted in Figure 4.8. The *Attune* program is also used for adjustment to compute the boresight angles and torsion.

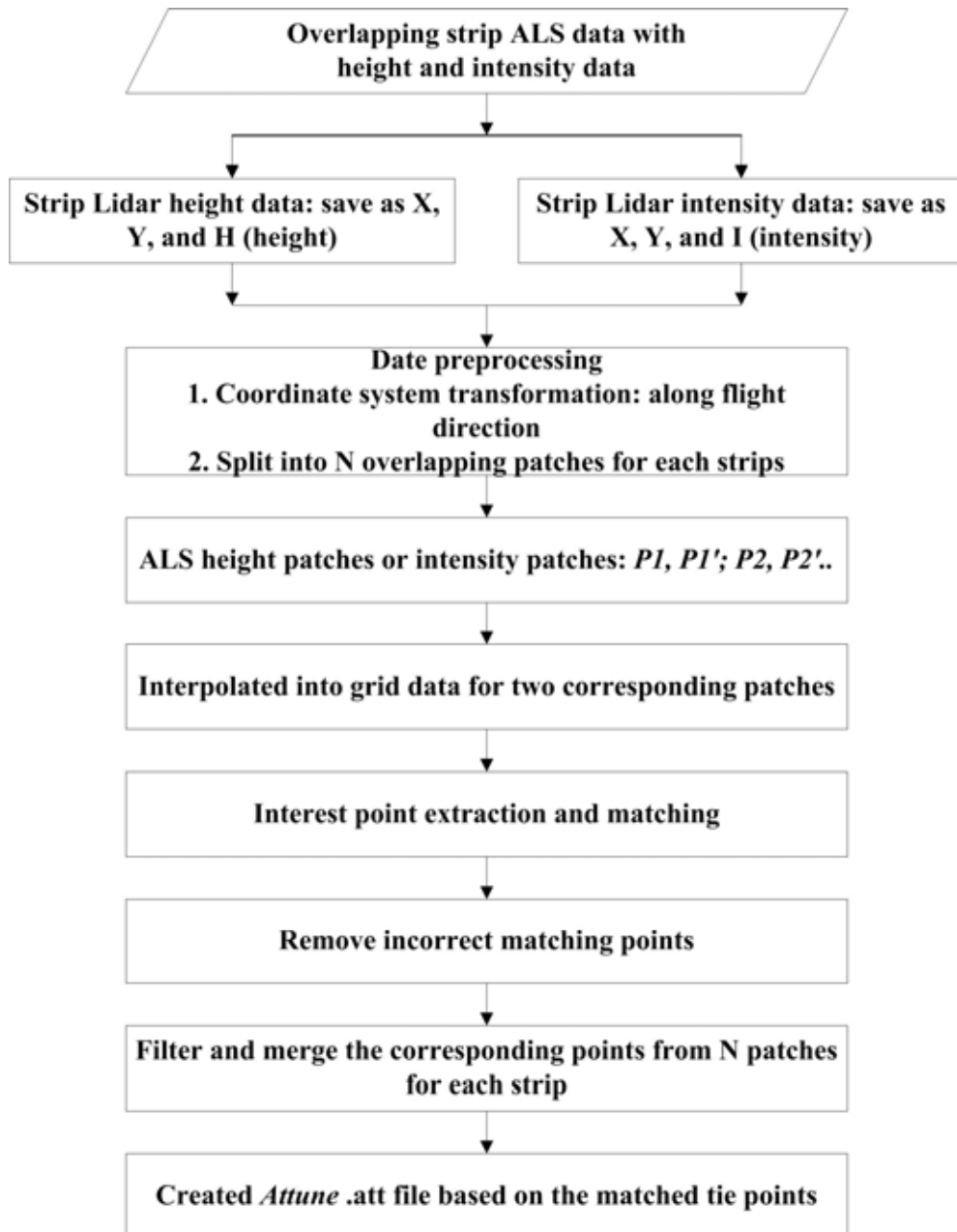


Figure 4.8: Work flow on the improvement of tie point selection for ALS calibration

4.1.5 Boresight calibration steps for the Optech ALTM

Although this research focuses on the Leica ALS system in examining the ALS boresight calibration, the current scheme on boresight calibration for the Optech ALTM system is introduced in this section. This part of the discussion follows a prior discussion on the current techniques on boresight calibration for the Optech ALTM system (see Section 2.3).

The order of the calibration parameters proceeds as follows: (1) *scanner offset correction*, (2) *pitch correction*, (3) *roll correction*, (4) *scale correction*, and (5) *TIMs (first/last pulse) correction* (CHSurvey, 2005). After calculating each calibration value, it is necessary to reprocess the data to check that the correction applied is correct.

(1) Scanner offset correction: First of all, calculating the scanner offset requires the use of two raw laser files from profile data. Calculate the average and the standard deviation of the offset column from these two raw files. Once the averages have been taken for the three strips, then take the average of the averages. The correction for the scanner offset will always be the opposite of the determined value. Its characteristics are stable enough so that the ALTM scarcely applies the scanner offset correction (Kao, 2005).

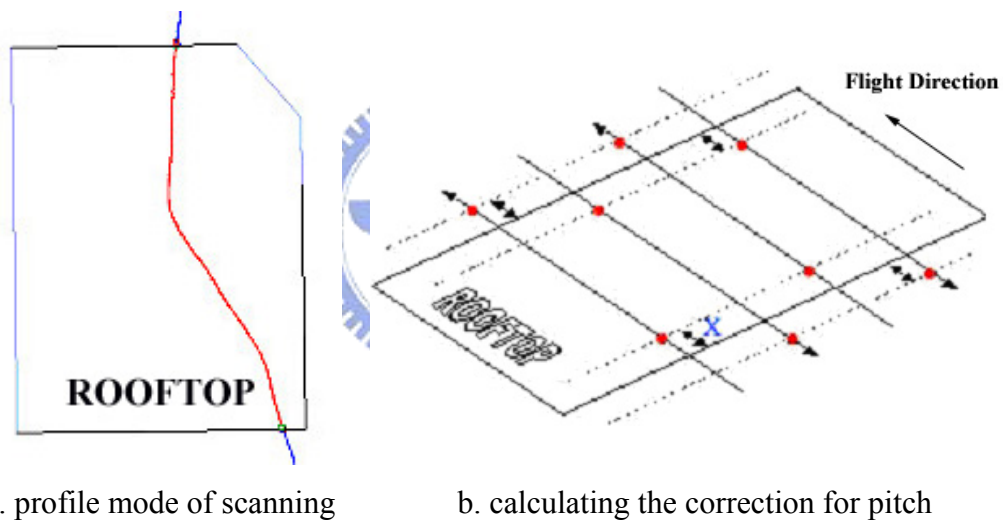


Figure 4.9: Profile mode of scanning and calculating the correction for pitch (CHSurvey, 2005)

(2) Pitch correction: Next, in calculating the correction for pitch, it is necessary to process the flight lines flown in profile mode (i.e. the frequency of oscillating mirror is 0, see Figure 4.9a) over the building. Take the average value of the first and the last pulse averages. This value is then divided by the height of the flight and multiplied by the inverse tangent (Figure 4.9b). This correction is then used to re-compute the laser points. This final step is to ensure that the correction for pitch has corrected the data. Convergence is reached whenever the correction is less than 0.01 degree.

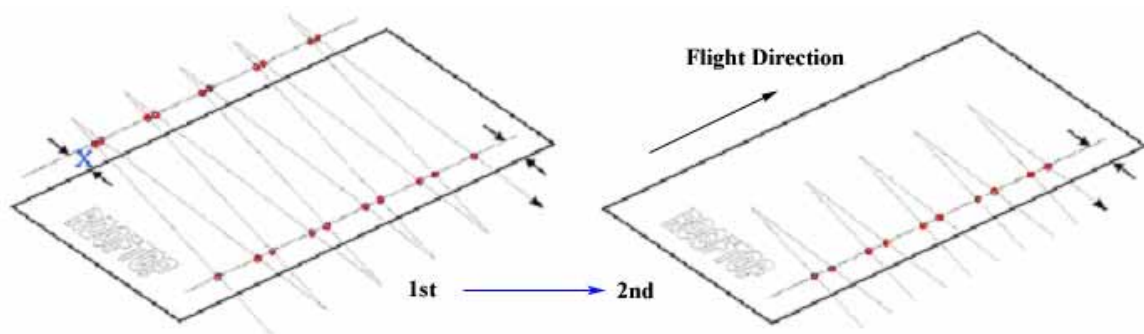


Figure 4.10: Calculating the correction for roll (CHSurvey, 2005)

(3) Roll correction: After the data are corrected for pitch, the next step is to calculate a value for roll. Roll correction involves, first, re-processing the scan data over the building. Take the average value of the first and the last pulse averages. This value is then divided by the height of the flight and multiplied by the inverse tangent (Figure 4.10). Similar to pitch correction, roll correction has an acceptable level of 0.01 degrees.

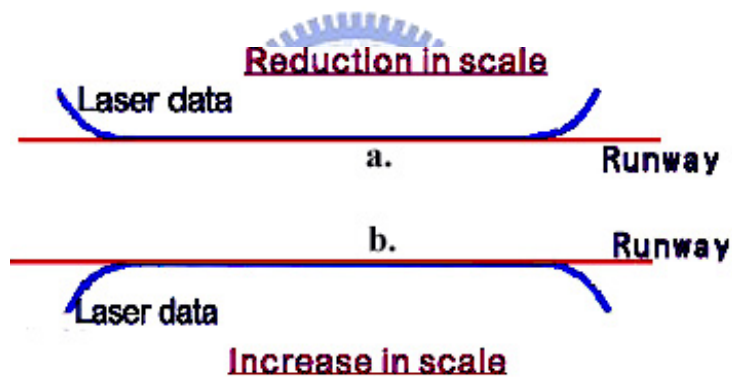


Figure 4.11: Scale effect along the profile of runway (Optech, 2003; CHSurvey, 2005)

(4) Scale correction: Next, in calculating the scale correction, process the runway data with all calibration parameters derived so far. Generate the output data per flight line so that each file contains only one strip. Determine which strip files contains the strips flown perpendicular to the runway. Activate the ground control points and one strip that was flown perpendicular to the runway. Draw a cross section along the length of the runway. If the cross section presented in Figure 4.11a looks like a smile, a reduction in scale needs to be applied to the data. If the cross section as shown in Figure 4.11b looks like a frown, an increase in the scale needs to be made to the data. To correct the data, measure the distance between the true

ground points and the laser data. Repeat the same measurements for other strips and average the measurements.

Finally, once corrections for scanner offset, pitch, roll, and scale have been determined and the laser data have been recomputed and the output generated, the TIMs correction (the first/last pulse correction, i.e. ranging correction) can then be determined. Find the ranging average for the first and last pulse points from runway data. The average values are used to compute the first pulse (T1) and last pulse (T2) range (Optech, 2003). If either of the T1 or T2 average values is negative, then the laser is ranging too long. A negative correction must be applied to increase the elevation data until they reach the same elevation as the control data. On the contrary, if either of the T1 or T2 average values is positive, then the laser is ranging too short. A positive correction must be applied to decrease the elevation data until they reach the same elevation as the control data.

Following the schemes described in this section, a practical boresight calibration data set derived from the Optech ALTM will be applied and demonstrated in Section 5.1.4.

4.2 Systematic error validation

Height offsets can be determined straightforwardly by comparing the heights of the horizontal planes. Planimetric offsets are more difficult to determine since edges cannot be precisely located due to the distance between neighboring laser points. In the case of an average point density with one point per square meter, an accurate location of details such as height jump edges is not possible to determine. One consequence of the determination of the edge location is that the interpolation is more or less involved. The interpolation of laser points to a regular grid may introduce severe systematic errors by creating non-existing points in case of partial occlusion (Maas, 2002). To avoid interpolating the raw laser points and to simultaneously evaluate the height and planimetry offsets from overlapping laser strips, a surface matching method is proposed in this research.

Systematic error validation is necessary for ALS data on two occasions. The first is to verify the calibrated data that are re-computed with updated calibration parameters from

calibration procedure. The other occasion is on demand for users who did not perform the calibration, or when the control information is insufficient for validation.

Most of the prior research on accuracy assessment for ALS data focused on height errors, as discussed in Section 2.4 and Section 3.1. Systematic planimetric errors are often much larger than height errors for ALS data, and therefore, a 3-D systematic error validation is the solution that delivers the most benefits.

A common problem in 3-D image analysis is the calculation of the transformation between two 3-D data sets. The transformation should be applied to one of the sets in order to match against the second set (Nikolaidis and Pitas, 2001). For example, when the measured data set needs to be matched, the sensor measurements need to correspond to a certain model. Registration methods are distinguished according to the type of geometric transformations and also on the basis of whether the correspondence between the matching points in the two data sets are known.

Besl and McKay (1992) presented a general-purpose, representation-independent method for registering a variety of 3-D shapes such as point sets, free form curves and surfaces (Besl and McKay, 1992; Nikolaidis and Pitas, 2001). In their method, registration between 3-D shapes related by the Euclidean transformation is carried out with an Iterative Closest Point (ICP) algorithm, which requires only a procedure to find the closest point on a geometric entity to a given point. A priori knowledge of the correspondence between points is not necessary.

Here a 3-D curve is used as an example. A general problem statement for the registration is posed as follows: given a set of 3-D points describing a data curve that may correspond to a model curve, and given a model curve in a model coordinate frame in an arbitrary shape representation, estimate the optimal rotation and translation that align the model and the data shapes. The representation of the model curve can be arbitrary, for example, it could be represented as a set of polylines (as normally done for natural lines). Some notions have to be explained before providing the details. A data curve P consisting of N_p points is transformed to be the best alignment with a model curve X with N_x line segments. The distance d between

a data point \vec{p} and a model curve X is denoted by $d(\vec{p}, X) = \min_{x \in X} \|\vec{x} - \vec{p}\|$ with the $\|\cdot\|$ symbol denoting the 3-D norm. The closest point on the model curve ($\vec{y} \in X$) is located for each point in $\vec{p} \in P$ to yield the resulting set of the closest points. Denoting that set by Y and the closest point operator by C , we can symbolically write an equation as the following: $Y = C(P, X)$. Given the resultant correspondence between the two point sets Y and P where each point \vec{p}_i corresponds to the point \vec{y}_i with the same index, our objective is to find a 3-D Euclidean transformation that minimizes the mean-squares error function.

$$f(T) = \frac{1}{N_p} \sum_{i=1}^{N_p} \|\vec{y}_i - T\vec{p}_i\|^2 = \frac{1}{N_p} \sum_{i=1}^{N_p} \|\vec{y}_i - R(\vec{q}_r)\vec{p}_i - \vec{q}_T\|^2 \quad (4-19)$$

where:

- T : denoting the 3-D Euclidean transformation in parameters $(X_0, Y_0, Z_0, \omega, \varphi, \kappa)$,
- R : representing the quaternion-based rotation vector,
- \vec{q}_R : representing the rotation vector $(\omega, \varphi, \kappa)$,
- \vec{q}_T : representing the translation vector (X_0, Y_0, Z_0) ,

and,

$$T(\vec{p}) = T \begin{pmatrix} p_x \\ p_y \\ p_z \end{pmatrix} = R(\omega, \varphi, \kappa) \begin{pmatrix} p_x - X_0 \\ p_y - Y_0 \\ p_z - Z_0 \end{pmatrix}$$

The cross-covariance matrix of P and Y can then be composed:

$$\Sigma_{py} = \frac{1}{N_p} \sum_{i=1}^{N_p} [(\vec{p}_i - \vec{u}_p)(\vec{y}_i - \vec{u}_y)^t] = \frac{1}{N_p} \sum_{i=1}^{N_p} [\vec{p}_i \vec{y}_i^t] - \vec{u}_p \vec{u}_y^t \quad (4-20)$$

where:

$$\vec{u}_p = \frac{1}{N_p} \sum_{i=1}^{N_p} \vec{p}_i \quad : \text{representing the gravity of } P,$$

$$\bar{u}_y = \frac{1}{N_y} \sum_{i=1}^{N_y} \bar{y}_i \quad : \text{representing the gravity of } Y,$$

The \bar{q}_R can be derived by applying the matrix singular value decomposition (SVD, *MATHWORKS*, 2004) based on Equation 4-20. The translation vector can then be computed:

$$\bar{q}_T = \bar{u}_y - R(\bar{q}_R)\bar{u}_p \quad (4-21)$$

This transformation is a subclass of a more general 3-D similarity transformation associated with an additional scale parameter. Given the corresponding point pair, the estimation procedure of the transformation T will be denoted by $T = Q(P, Y)$. The ICP algorithm can now be stated. Given the point set P with N_p points and the model curve X with N_x line segments, along with initial values $T^0 = (X_o^0, Y_o^0, Z_o^0, \omega^0, \phi^0, \kappa^0)$ of the Euclidean 3-D transformation parameters, the following steps are applied iteratively starting with $P^0 = T^0(P)$ until convergence within a tolerance τ (Besl and McKay, 1992; Hajnal et al., 2001; Lin, 2002). The worst computational costs of each operation are given in brackets.

- Compute the set of closest points: $Y^K = C(P^K, X)$ [cost: $O(N_p N_x)$].
- Estimate the transformation parameters: $T^K = C(P^K, Y^K)$ [cost: $O(N_p)$]
- Apply the transformation T^K to update the positions of the transformed data point set via $P^{K+1} = T^K(P^K)$ [cost: $O(N_p)$].
- Check the change in the mean-squares error and terminate the iterations when it falls below a predefined threshold τ , that is, $f(T)^{K+1} - f(T)^K < \tau$, $\tau > 0$.

In short, the data set $\{p_i\}$ is transformed by the transformation T which is iteratively established from a correspondence between the points $\{p_i\}$ and those points on the model curve (y_i) that happen to be the closest to the set P transformed with the transformation

parameters estimated in the previous iteration (T^K). The idea driving the ICP algorithm is illustrated in Figure 4.12 (Lin, 2002).

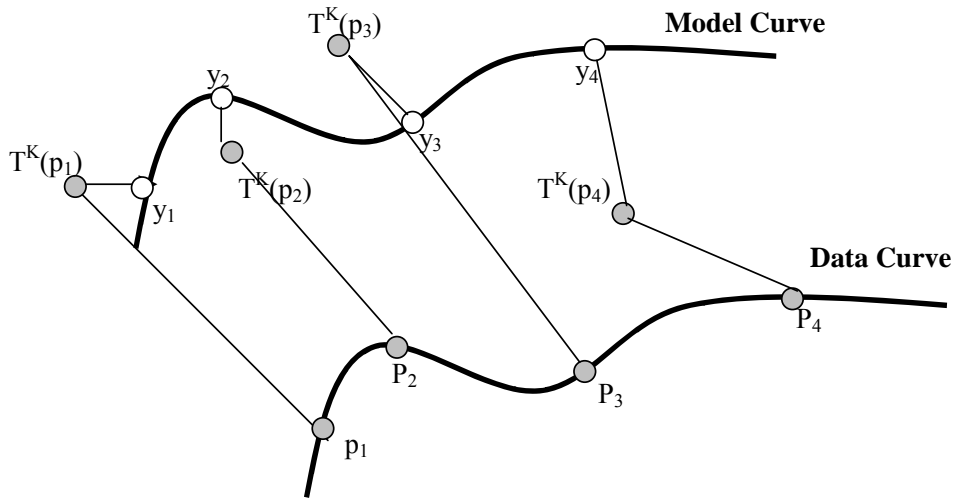


Figure 4.12: The ICP algorithm

A practical 2-dimensional example for the ICP algorithm as shown in Figure 4.13 is generated with the demo program provided by Chui & Rangarajan (2003). The measured point set P needs to be matched to data set X . Figure 4.13a presents the original position/shape of measured point set (P) and data point set (X). Next, the changed position/shape of measured points set (P) with i^{th} iteration is shown in Figure 4.13b while the change in mean-squares error is about 0.125. The final position/shape of measured points set (P) is depicted as Figure 4.13c while the change in mean-squares error falls below 0.001.

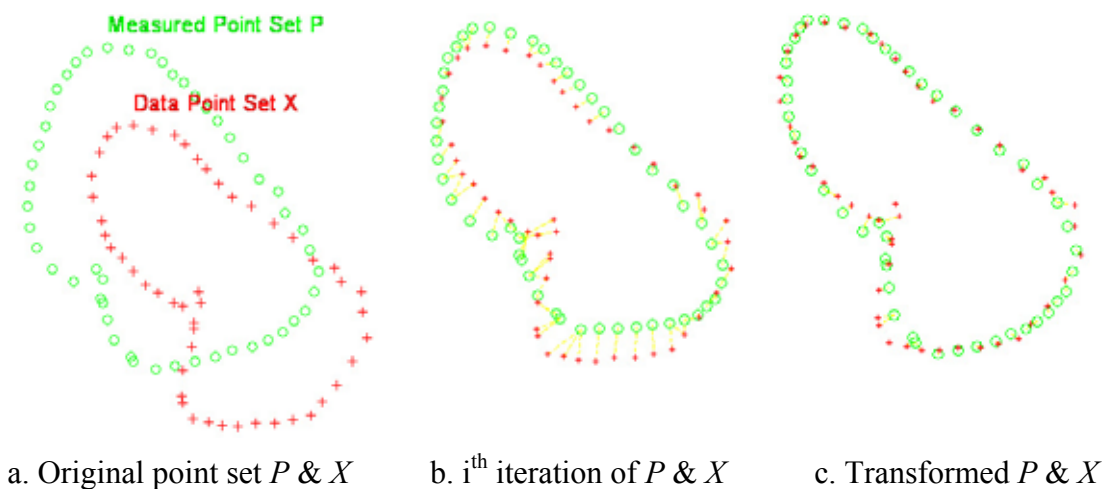


Figure 4.13: A practical example for the ICP algorithm operation

4.3 Remaining systematic error recovery

The definition of “recovery” here is to recover the laser strips that have systematic errors. Most of the data users will require point clouds that are referenced against a mapping frame, or ask for DSM/DTM generated from ALS point clouds. Usually, for the POS (position and orientation) data, base station surveying data and raw laser scanning data are not available for most users. Therefore, it is impossible to re-process the laser points when the data have systematic errors. A variety of procedures have been developed to recover the laser strips that have systematic errors by applying photogrammetric methodology. An example is strip adjustment (see Section 3.1 for literature review).

The ICP algorithm not only play a successful role to estimate the planimetry shifts and height offsets from overlapping laser scanning strips, but also recover the imperfect data set based on the reference data set. Nevertheless, it is not possible to apply the ICP algorithm to two adjacent strips, due to time and computation memory constraints.

In this research, two easily implemented methods are proposed to recover ALS strips. The first method is the 3-D similarity transformation, which is a common approach to register the laser points and eliminate systematic errors (Crombaghs et al., 2000; Maas, 2000). The laser points coming from two neighboring strips form two Cartesian reference systems that are different from one another by translation, rotation and scale, although the scale factor is usually assumed to be unity. This method is applicable when the ground control information is not available.

The 3-D similarity transformation is also known as the seven-parameter transformation (Mikhail et al., 2001). It transfers points from one 3-D coordinate system (xyz), to another (XYZ). This transformation involves seven parameters - three rotation, three translation, and one scale factor, To develop the equations, imaging an $x'y'z'$ coordinate system that is parallel with XYZ , but whose origin is common with the origin of the xyz system. The three sequential 2D rotation that follow - α , β , and γ , convert coordinates from $x'y'z'$ to xyz .

Each of the three elementary rotations is represented in a matrix form as follows:

$$\begin{bmatrix} x' \\ y' \\ z' \end{bmatrix} = \begin{bmatrix} 1 & 0 & 0 \\ 0 & \cos \omega & \sin \omega \\ 0 & -\sin \omega & \cos \omega \end{bmatrix} \begin{bmatrix} x \\ y \\ z \end{bmatrix} = M_\omega \begin{bmatrix} x \\ y \\ z \end{bmatrix} \quad (4-22a)$$

$$\begin{bmatrix} x'' \\ y'' \\ z'' \end{bmatrix} = \begin{bmatrix} \cos \phi & 0 & -\sin \phi \\ 0 & 1 & 0 \\ \sin \phi & 0 & \cos \phi \end{bmatrix} \begin{bmatrix} x' \\ y' \\ z' \end{bmatrix} = M_\phi \begin{bmatrix} x' \\ y' \\ z' \end{bmatrix} \quad (4-22b)$$

$$\begin{bmatrix} x''' \\ y''' \\ z''' \end{bmatrix} = \begin{bmatrix} \cos \kappa & \sin \kappa & 0 \\ -\sin \kappa & \cos \kappa & 0 \\ 0 & 0 & 1 \end{bmatrix} \begin{bmatrix} x'' \\ y'' \\ z'' \end{bmatrix} = M_\kappa \begin{bmatrix} x'' \\ y'' \\ z'' \end{bmatrix} \quad (4-22c)$$

The three rotations in Equation (4-22) are often referred to as elementary rotations, since they may be used to construct any required set of sequential rotation. By successive substitution, the total rotation matrix is obtained:

$$Y = M_\kappa M_\phi M_\omega X = MX \quad (4-23)$$

$$Y = [x''' \ y''' \ z''']^t, \quad X = [x \ y \ z]^t \quad (4-24)$$

$$M = \begin{bmatrix} \cos \phi \cos \kappa & \cos \omega \sin \kappa + \sin \omega \sin \phi \cos \kappa & \sin \omega \sin \kappa - \cos \omega \sin \phi \cos \kappa \\ -\cos \phi \sin \kappa & \cos \omega \cos \kappa - \sin \omega \sin \phi \sin \kappa & \sin \omega \cos \kappa + \cos \omega \sin \phi \sin \kappa \\ \sin \phi & -\sin \omega \cos \phi & \cos \omega \cos \phi \end{bmatrix} \quad (4-25)$$

$$M = \begin{bmatrix} m_{11} & m_{12} & m_{13} \\ m_{21} & m_{22} & m_{23} \\ m_{31} & m_{32} & m_{33} \end{bmatrix} \quad (4-26)$$

The general form of 3-D similarity transformation can be derived:

$$Y = \lambda MX + t \quad (4-27)$$

with λ , a uniform scale change, three rotation ω , ϕ , and κ , and three translations, $t=[t1 \ t2 \ t3]$. With the correspondence derived from two neighboring strips by applying ICP matching, it can be used as the tie point to solve the seven parameters. In order to obtain the best solution,

a least-squares adjustment is utilized again. Therefore, the seven parameters are used to adjust the strip that has systematic error.

The second method is the strip adjustment with three-parameters - a strip adjustment procedure concerning the heights. The method originated from Crombaghs et al. (2000) and it was discussed in Section 3.1. The testing program for this method is provided by Tung (2005). Both the first and the second method are used in this research.

4.4 ALS data preprocessing

To improve the accuracy of calibration, systematic error validation, and ALS remaining systematic error recovery, ALS data are usually passed through a series of initial filters to remove outliers. Filtering is critical to ensure the accuracy of tie points. These filters typically analyze individual points and compare them to their immediate neighbors with a certain searching radius. If the difference in elevation is large, such as being lower than 0.5 meters, then the individual point is removed. This procedure is very effective at removing outliers. These outliers are usually classified as low-point levels, according to the classification procedures listed in *TerraScan* (Soininen, 2004). This fundamental procedure to check and remove distinct gross errors is also applied to planimetry records for each strip.

Next, the magnitude of the coordinate values also posed a numerical problem for a personal computer (PC) – large number begin to lose precision with only 8 bytes to store them. The solution was to transform the coordinate system of ALS data into a local strip coordinate frame (Figure 3.1) based on an affine transformation.

4.5 Test data

Test data selection depends on the tasks of this research. Firstly, there is a standard test sets with four flight lines derived from a calibration site. Next, two test sites are used for systematic error validation. The reasons to select these two sites are that both of them present significant systematic errors from previous work. In the end, these two test sites, which are applied in systematic error validation, are also applied to data adjustment.

4.5.1 ALS boresight calibration

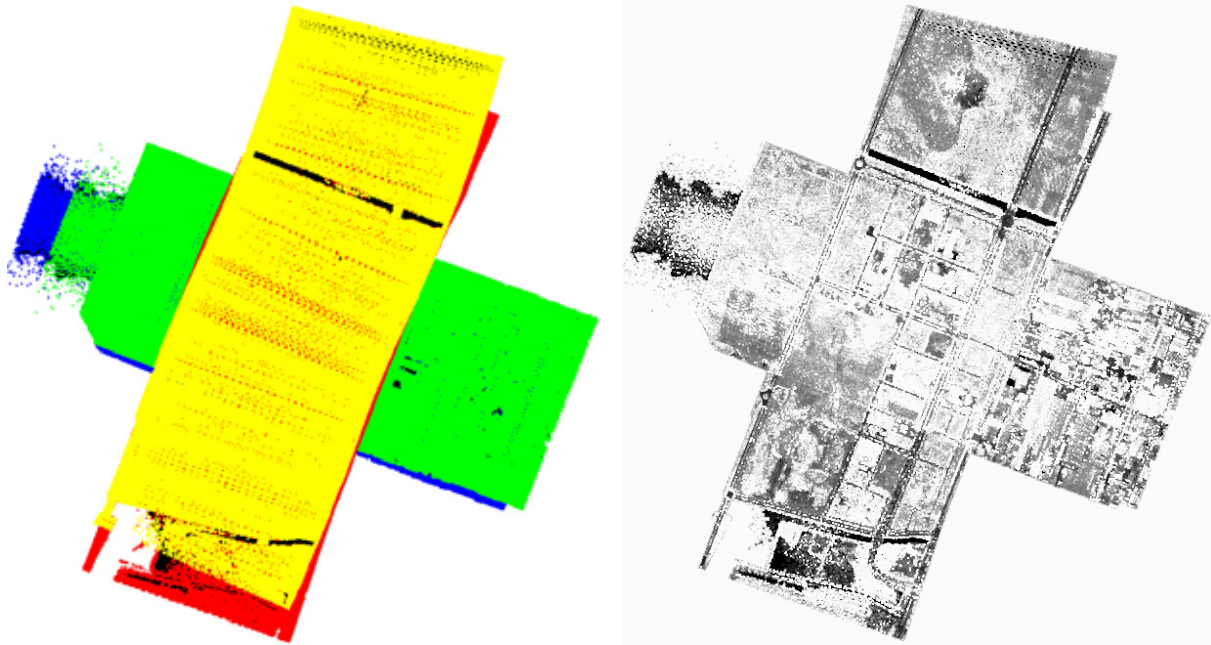
Table 4.1: Flight parameters of boresight calibration

Parameter	Value
Pulse rate	47.6 kHz
Scan rate	34.1 Hz
Returns/intensities	1/1
Operating altitude (AGL)	600 m/1000 m
FOV	45 degree
Aircraft speed	125 knots

The test data for ALS boresight calibration is captured from a calibration site (Figure 4.14) locating in Taichung, Taiwan (ITRI, 2004 & 2005). The ALS flight parameters are depicted in Table 4.1. The flat area with minor terrain variation and low percentage vegetation covering is the most significant criterion for choosing an ALS calibration site. Next, there should be some easily identifiable ground features to select as tie points. The dimension of this calibration site is about 1 km by 1 km. Two perpendicular roads in the center area have been manually surveyed as ground check points by using an automatic level. There are 520 points to collect at regular intervals along these two perpendicular roads.

The calibration data were captured in the cloverleaf pattern described in Section 4.1.2, with flight directions altering on each pass and at 2 different altitudes. To have the discrepancies between strips overemphasized, the incorrect calibration angles and torsion will apply to *ALS Post Processor* program (Leica, 2004b). The *ALS Post Processor (PP)* is the main tool for combining the collected IMU positioning and GPS data with the raw collected ALS data. The operation of the ALS PP takes the smoothed best positioning solution (SBET) measured to the optical center of the instrument and the ranging and other associated laser information and determines the position of the point clouds in the mapping frame (Leica, 2003; Leica, 2004b).

The point clouds and intensity of the calibration strips are shown in Figure 4.14a and Figure 4.14b, respectively. Except the boresight calibration strips, four more strips were taken as the validation data with different flight parameters. These flight parameters will therefore apply to the practical ALS missions (ITRI, 2004 & 2005).



a. Point clouds

b. Intensity data

Figure 4.14: The point clouds and intensity of the calibration strips

4.5.2 System data validation

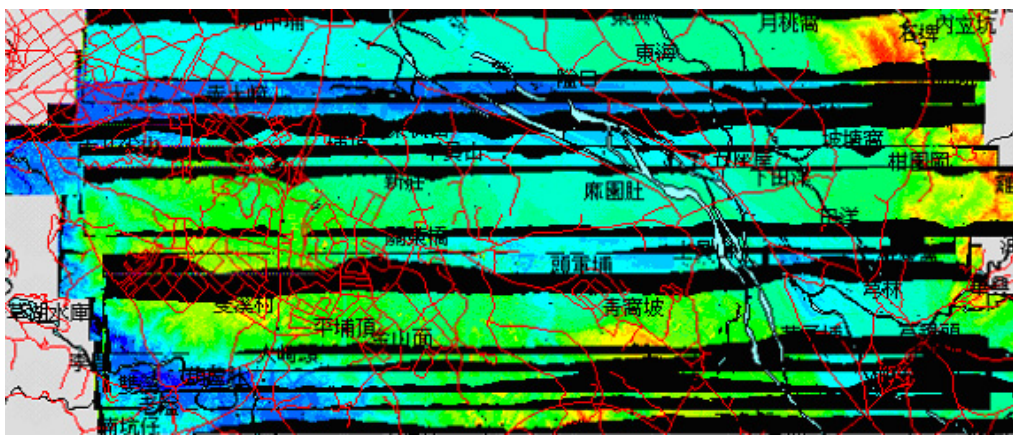
Table 4.2: Technical parameters of the airborne laser scanning data for test sites.

Parameters	Test site I (<i>SI</i>)	Test site II (<i>SII</i>)
Sensor type	Leica ALS40	Leica ALS50
Range	800m	1500m
Scan rate	25 khz	57.6 khz
Pulse rate	38 khz	74.7 khz
FOV	35°	58°
Aircraft speed	125 knots	125 knots
Avg. ground swath	650m	1,150m
Total strips	19	> 60
Location	Hsinchu/Taiwan	Kaoping/Taiwan
Operating date	April 2002	October 2004
Average density	0.55 pts/m ²	0.90 pts/m ²

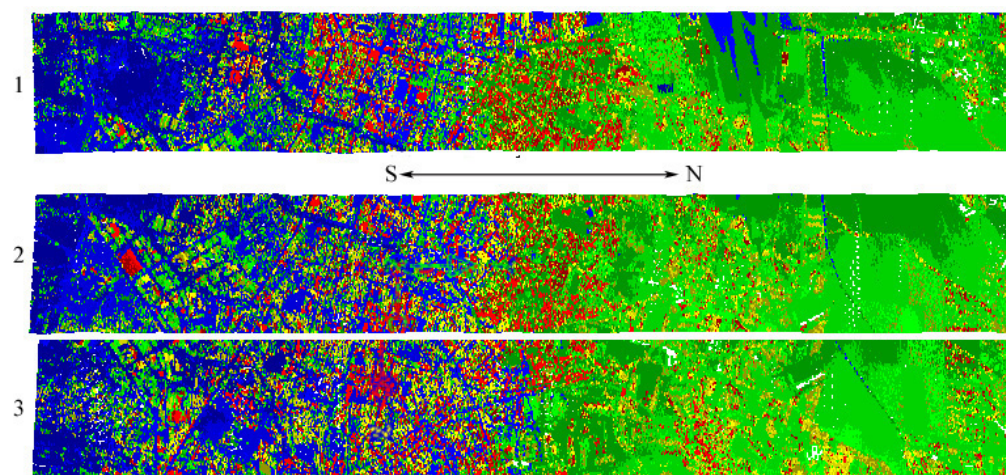
To evaluate the performance of proposed surface matching method for laser data of different quality, two data sets are selected for experiments in this research. The technical details of these two test sites are summarized in Table 4.2. Test data I has height discrepancies up to 1.6 m according a previous analysis (Shih and Peng, 2003). Test data II is derived from another ALS surveys. More than sixty flight lines were taken for this survey. Only three of

them are chosen for validation. According to the project's report, the height offsets can sometimes reach 40 cm for some strips (ITRI, 2005). The data sets with naturally existing systematic errors, like test data I, are suitable for this research.

These two sites will be abbreviated as *SI* and *SII* in the remaining parts of this dissertation. *SI* (Figure 4.15a) consists of suburban settlement and agriculture land, and has the average ground height difference of 200 m. *SII* (Figure 4.15b) covers urban, suburban, and farmland, and has the smaller terrain variation with a ground height range of 70 m. For test data *II*, the laser points in the coordinate system of mapping frame are computed with the boresight misalignment parameters which were determined in this research (i.e. the parameters derived from Section 5.1). Therefore, the experimental result for *SII* can also evaluate the accuracy of the boresight misalignment parameters.



a. Test site I



b. Test site II

Figure 4.15: Two test sites for systematic error validation

The height offsets of *SI* and *SII* are evaluated by using ground control information for a preliminary check before applying surface matching. The computed height statistics are list in Appendix B for *SI* and *SII*. Some points that present unreasonable elevation should be removed before further processing. For example, strip 1 and strip 4 in *SI*, strip 1 and strips 2 in *SII* have outliers with negative elevation values. These outliers can be easily removed by classifying them as the “low points” level in *TerraScan* (Soininen, 2004). This procedure to check and remove distinct gross errors is also applied to the planimetry records for each strip.

According to Shih and Peng’s study (2003), they found height offsets between the 9th strip and the 10th strip in *SI*. The magnitude is estimated to be up to 1.6 m. A preliminary analysis is performed to check the height offsets in both test data sets. The ground control points (GCPs), obtained with field GPS-RTK, is used to check the height offsets for each strips for *SI* and *SII*.

The comparison is based on two data sets in (X, Y, Z) triplet format from laser scanning points and GCPs, respectively. Due to the different point spacing of two data sets, a search criterion is needed to find the ‘same’ point from these two files. In this study, the search criterion is set to be 1.0 m. Based on this criterion, two points from different DSM data sets with a distance less than 1.0 m are considered as ‘identical’ points. Next, the elevation difference between the two identical points is computed. The statistics of height differences between laser scanning points and GCPs are presented in Appendix C and depicted as Figure 4.13.

$$\text{Difference } \Delta Z_i = Z_i - Z_i^0 \quad (4-28)$$

Z_i^0 : elevation from the laser scanning data

Z_i : elevation from the GCP with corresponding to laser scanning data

$$\text{Mean } \overline{\Delta Z} = \left(\sum_{i=1}^n \Delta Z_i \right) / n \quad (4-29)$$

$$RMSE = \sqrt{\left(\sum_{i=1}^n \Delta Z_i^2 \right) / n} \text{ (root mean square error)} \quad (4-30)$$

$$\sigma = \sqrt{\frac{\sum_{i=1}^n (\Delta Z_i - \overline{\Delta Z})^2}{n-1}} \text{ (standard deviation)} \quad (4-31)$$

The results show that height offsets exist in strip laser scanning data (see Appendix C and Figure 4.16). For test site I (*SI*), the mean height offsets range from -0.23 m to 0.12 m across strips 1 to 9. On the contrary, the mean height discrepancies range from -1.42 m to -2.06 m across strips 10 to 18. The mean height differences range from -0.13 m to 0.33 m, while the standard deviation is consistently less than 12 cm for all strips in *SII*. The average height difference of strip 1 is much higher than the other strips. The result suggests that strip 1 need to be further validated. Based on the unique calibration and flight parameters in an ALS survey, the accuracy of point clouds for the computed coordinates should be considered as a coincidence. Like strip 1, a review of the quality assessment indicates that there are a few flight lines presenting higher average height offsets (ITRI, 2005). It reveals that the remaining systematic errors are present occasionally, even though the system has been well-calibrated.

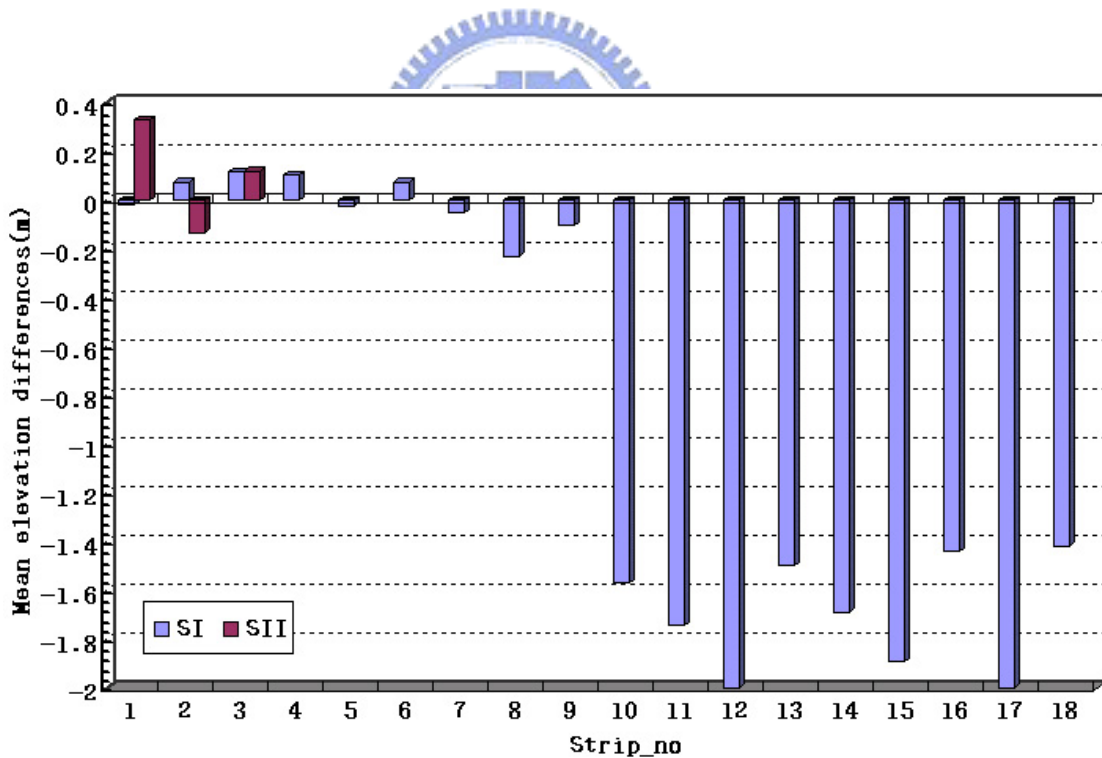


Figure 4.16: The average of height differences between laser points and GCPs for *SI* and *SII*

The best way to recover the significant height offsets from strips 10 to 19 of *SI* is to reprocess the GPS, IMU, and laser range data. The magnitude of height discrepancies reach

1.6 m, and this is much worse than the predicted accuracy, i.e. 15 cm, at its flight attitude (Optech, 2002; Leica, 2002). However, in most cases, the packages and GPS/IMU as well as the raw range data are not available to general users. This research proposes a surface matching method dealing with laser points that is applied to some strips in estimating the height offsets as well as planimetry shifts.

4.5.3 Remaining systematic error recovery

Basically, a strip adjustment is applied to the ALS data that have systematic errors. The necessity for applying the adjustment to laser data depends on the applications of ALS. For example, it is definitely not necessary to produce DTMs with low resolution from ALS data. However, large-scale city model will need adjustments to ensure higher data accuracy. Once the boresight misalignment parameters, i.e. roll, pitch, heading, torsion and z shift, are well calibrated, the computed coordinate to each strip should have no systematic errors. Nevertheless, according to the report of ITRI (2005), the average height discrepancies in some strips are more than 15 cm.

The test sites used in systematic error validation are also used in the remaining systematic error recovery. The experimental results for applying a 3-D similarity transformation and a strip adjustment with three-parameters to these two test data are presented in Section 5.3.